Stochastic Dynamics of Skyrmions on a Racetrack: Impact of Equilibrium and Nonequilibrium Noise

Anton V. Hlushchenko¹, Mykhailo I. Bratchenko¹, and Aleksei V. Chechkin^{1,2,3*}

¹National Science Center "Kharkiv Institute of Physics and Technology", 61108 Kharkiv, Ukraine

²Max Planck Institute of Microstructure Physics, 06120 Halle, Germany and

³Faculty of Pure and Applied Mathematics, Wrocław University of Science and Technology, 50-370 Wrocław, Poland

(Dated: November 26, 2025)

Current-driven motion of domain walls and skyrmions is central to the operation of non-volatile magnetic memory devices. Racetrack memory requires current densities high enough to generate velocities above 50 m/s, but such conditions also enhance spin-current noise. We develop a theoretical framework based on the stochastic Thiele equation to analyze the effects of equilibrium (thermal) and nonequilibrium (spin-current) fluctuations on skyrmion dynamics. From this approach, we derive diffusion coefficients and mean-squared displacements that quantify stochastic motion under both noise sources. Micromagnetic simulations and analytical results demonstrate that spin-current noise dominates skyrmion dynamics in typical racetrack structures up to room temperature. We further address the first-passage-time problem, obtaining the mean first-passage time and its standard deviation along and across the racetrack. These results quantify how random displacements affect skyrmion propagation and detection, providing insights into error sources in high-speed racetrack memory devices.

Developments in the controlled motion of magnetic textures, such as domain walls on racetracks driven by electric currents, have opened the way to alternative non-volatile memory devices with significantly higher performance than conventional solid-state memories [1]. Advances in racetrack memory technology now enable a wide range of applications, from ultra-fast to ultra-dense data storage [2, 3].

An alternative to domain-wall magnetic textures is the skyrmion [4], which can provide denser information storage due to its nanoscale size (down to a few nanometers). These particle-like spin configurations can exist either in magnetic materials with non-centrosymmetric crystal lattices or at the interfaces of magnetic films. Correspondingly, two types of skyrmion states arise from different forms of the Dzyaloshinskii–Moriya interaction (DMI). In non-centrosymmetric lattices [5–7], the bulk DMI stabilizes vortex-like (Bloch-type) skyrmions [8]. In contrast, interfacial DMI leads to the stabilization of "hedgehog" (Néel-type) skyrmions [9, 10]. Moreover, Néel-type skyrmions can also be stabilized in centrosymmetric ferromagnets by imposing a vertical strain gradient via epitaxial growth [11].

Historically, the first racetrack memories were realized in permalloy nanowires [1], where domain walls were driven by nanosecond current pulses via the spin-transfer torque (STT) mechanism [12–15]. The next generation of racetracks [2, 16, 17] was achieved by injecting a spin current from a heavy-metal layer into an adjacent ferromagnetic layer. The resulting spin-current—induced motion of the magnetic texture arises from spin—orbit scattering of conduction electrons via the spin Hall effect in the heavy-metal layer [18–20] and is described by the spin—orbit torque (SOT) mechanism. In this work, we focus on racetracks with SOT current injection, which

enables higher velocities of magnetic textures. However, our theoretical framework can be readily extended to the STT case.

Real magnetic systems are inherently subject to random fluctuations, which may include both equilibrium and nonequilibrium sources of noise. Equilibrium thermal agitation leads to fluctuations of the magnetization field [21–29]. In contrast, the presence of an external current gives rise to nonequilibrium noise [30–40]. In highspeed spintronic devices (with typical velocities of at least about 50 m/s or higher [2, 41-43]), large current densities can lead to enhanced spin-current fluctuations. In conventional electrical conductors, such as heavy-metal layers interfaced with nanoscale ferromagnets, spin-current noise increases magnetization noise through fluctuating spin torque [34, 40]. Anomalous behavior of magnetization fluctuations in current-controlled spin valves has already been demonstrated at cryogenic temperatures [44], and this effect is expected to remain significant even at room temperature.

One of the major technological challenges in racetrack memory is achieving the highest possible packing density of nanoscale magnetic textures [45–47], while still enabling reliable detection of domain walls or skyrmions when they are densely packed. In this work, we focus on describing the effects of both thermal noise and spin-current noise on skyrmion dynamics. Our results reveal a pronounced impact of spin-current fluctuations on the stable operation of racetrack memory devices. For typical racetrack geometries and operational conditions, trajectory offsets caused by spin-current noise dominate over thermal noise. This stochastic spreading of skyrmion trajectories is quantified in terms of the mean squared displacement (MSD), which we obtain analytically using the Thiele approach and numerically through micromag-

netic simulations. We also address the first-passage-time (FPT) problem for skyrmion motion on the racetrack, estimating the mean and standard deviation of the random times at which a skyrmion reaches either the racetrack side boundary or the detection region. Interaction of a skyrmion with a boundary can lead to its annihilation [48] and consequent loss of stored information, thereby compromising racetrack stability. Conversely, time uncertainty in reaching the detection region affects signal decoding quality. A deeper understanding of the roles of equilibrium and nonequilibrium fluctuations in skyrmion motion is therefore essential for the design of next-generation, high-speed, and high-density spintronic devices.

The dynamics of magnetization $\mathbf{M}(\mathbf{r},t) = (M_1(\mathbf{r},t), M_2(\mathbf{r},t), M_3(\mathbf{r},t))$ is described by the Landau-Lifshitz-Gilbert (LLG) equation [49, 50], which includes additional term accounting for the spin transfer moment:

$$\partial_t \mathbf{M} = -\gamma \mathbf{M} \times \mathbf{H}_{\text{eff}} + \frac{\alpha}{M_s} \mathbf{M} \times \partial_t \mathbf{M} + \mathbf{T}_{\text{SOT}}.$$
 (1)

Here \mathbf{H}_{eff} is the effective field, γ is the gyromagnetic ratio, α is the damping parameter, M_s is the saturation magnetization. The spin-orbit torque \mathbf{T}_{SOT} can be expressed as a combination of Slonczewski's torque [12] and the damping-like torque:

$$\mathbf{T}_{SOT} = -\frac{\gamma}{M_s^2 \mathcal{V}} \mathbf{M} \times (\mathbf{M} \times \mathbf{I}_s) - \frac{\gamma \beta}{M_s \mathcal{V}} \mathbf{M} \times \mathbf{I}_s, \quad (2)$$

where $\mathbf{I}_s = \mathbf{P}I\hbar/(2e)$ ($\mathbf{P} = P \cdot \mathbf{p} = P \cdot (\cos \psi, \sin \psi, 0)$) the spin-polarization vector, \hbar the reduced Planck constant, e the electron charge, I the electric current, β the amplitude of the damping-like torque, and \mathcal{V} the sample volume.

Next, we generalize the LLG equation to account for both thermal noise and spin-current noise. Following Ref. [21], the thermal noise is represented by a fluctuating magnetic field $\delta \mathbf{h}(\mathbf{r},t)$ with zero mean as $\mathbf{H}_{\text{eff}} \to \mathbf{H}_{\text{eff}} + \delta \mathbf{h}$. In addition to the thermal noise, by analogy with Ref. [36], we introduce spin-current noise $\delta \mathbf{I}(\mathbf{r},t)$ as $\mathbf{I}_s \to \mathbf{I}_s + \delta \mathbf{I}$. This form of noise is analogous to the charge shot noise [51]. The discrete nature of the electron transport in the heavy metal leads to stochastic angular-momentum transfer between conduction electrons and atomic spins in the ferromagnetic layer [34, 38]. The stochastic LLG equation reads as

$$\partial_{t}\mathbf{M} = -\gamma\mathbf{M} \times (\mathbf{H}_{\text{eff}} + \delta\mathbf{h}) + \frac{\alpha}{M_{s}}\mathbf{M} \times \partial_{t}\mathbf{M}$$
$$-\frac{\gamma}{M_{s}^{2}\mathcal{V}}\mathbf{M} \times (\mathbf{M} \times (\mathbf{I}_{s} + \delta\mathbf{I})) - \frac{\gamma\beta}{M_{s}\mathcal{V}}\mathbf{M} \times (\mathbf{I}_{s} + \delta\mathbf{I}).$$
(3)

The autocorrelation functions of fluctuation terms take

the form [21, 34, 40]

$$\langle \delta h_i(t, \mathbf{r}) \delta h_j(t', \mathbf{r}') \rangle = \frac{2\alpha k_B T}{\gamma M_s} \delta_{ij} \delta(\mathbf{r} - \mathbf{r}') \delta(t - t'),$$

$$\langle \delta I_i(t, \mathbf{r}) \delta I_j(t', \mathbf{r}') \rangle = \frac{\alpha M_s \mathcal{V}^2}{\gamma} \delta_{ij} \delta(\mathbf{r} - \mathbf{r}') \delta(t - t') \quad (4)$$

$$\times \frac{\delta \varepsilon}{E_F} (eU \coth \frac{eU}{2k_B T} - 2k_B T).$$

Here $i, j = \{x, y, z\}$, δ_{ij} is the Kronecker delta function, $\delta(\cdot)$ is the Dirac delta function, U and T denote the applied voltage and temperature, E_F is the Fermi energy in the heavy-metal layer, $\delta \varepsilon$ is the exchange splitting in the ferromagnetic layer, which can be estimated as $\delta \varepsilon \sim E_F/5$ [34]. We consider equilibrium and nonequilibrium noise sources of different origins, assuming that they are uncorrelated, $\langle \delta h_i(t, \mathbf{r}) \delta I_j(t', \mathbf{r}') \rangle = 0$. In the zero temperature limit, the current fluctuations persist, while in the absence of an applied voltage, only thermal fluctuations remain.

We employ the Thiele approach to evaluate the contribution of equilibrium and nonequilibrium noise to skyrmion displacements. The Thiele formalism [52] uses the traveling-wave Ansatz $\mathbf{M}(\mathbf{r},t) = \mathbf{M}(\mathbf{r} - \mathbf{R}(t))$, where $\mathbf{R}(t)$ is the position of the center of skyrmion. In our study, we neglect the higher derivatives of $\mathbf{R}(t)$ [53], which have only a minor effect on the main results, and reduce Eq. 3 to the form of the stochastic Thiele equation (see details in the Supplemental Material, Section I)

$$\widehat{G} \cdot \dot{\mathbf{R}} + \alpha \widehat{D} \cdot \dot{\mathbf{R}} + \mathbf{F} = 0,$$

$$\mathbf{F} = \mathbf{F}_{eff} + \mathbf{F}_{SOT} + \mathbf{F}_{\delta h} + \mathbf{F}_{\delta I},$$
(5)

where \widehat{G} is the gyrotropic tensor and \widehat{D} is the dissipation tensor, which are given by $G_{ij} = -1/(\gamma M_s^2) \int \mathbf{M} \cdot (\nabla_i \mathbf{M} \times \nabla_j \mathbf{M}) d\mathbf{r}$ and $D_{ij} = 1/(\gamma M_s) \int \nabla_i \mathbf{M} \cdot \nabla_j \mathbf{M} d\mathbf{r}$, respectively. The effective force is $F_{eff,i} = \int \mathbf{H}_{eff} \cdot \nabla_i \mathbf{M} d\mathbf{r}$, and $F_{\text{SOT},i} = 1/(\gamma M_s^2) \int (\mathbf{M} \times \nabla_i \mathbf{M}) \cdot \mathbf{I}_s d\mathbf{r} + \beta/(\gamma M_s) \int \mathbf{I}_s \cdot \nabla_i \mathbf{M} d\mathbf{r}$. The two uncorrelated stochastic forces take the form

$$F_{\delta I,i} = \frac{1}{\gamma M_s^2} \int (\mathbf{M} \times \nabla_i \mathbf{M} + M_s \beta \nabla_i \mathbf{M}) \cdot \delta \mathbf{I} d\mathbf{r},$$

$$F_{\delta h,i} = \int \delta \mathbf{h} \cdot \nabla_i \mathbf{M} d\mathbf{r},$$
(6)

and their autocorrelation functions are given by

$$\langle F_{\delta h,i}(t)F_{\delta h,j}(t)\rangle = \alpha k_B T D_{ij}\delta(t-t'),$$

$$\langle F_{\delta I,i}(t)F_{\delta I,j}(t)\rangle = \alpha (1+\beta^2)D_{ij}\delta(t-t')$$

$$\times \frac{\delta \varepsilon}{E_F}(eU \coth \frac{eU}{2k_B T} - 2k_B T).$$
(7)

The resulting Eqs. (5)-(7) describe two-dimensional skyrmion diffusion in thin ferromagnetic films in the (x-y) plane. Owing to the rotational symmetry of a skyrmion at rest we neglect D_{xy} and D_{yx} , and set $D_{xx} = D_{yy} = D$

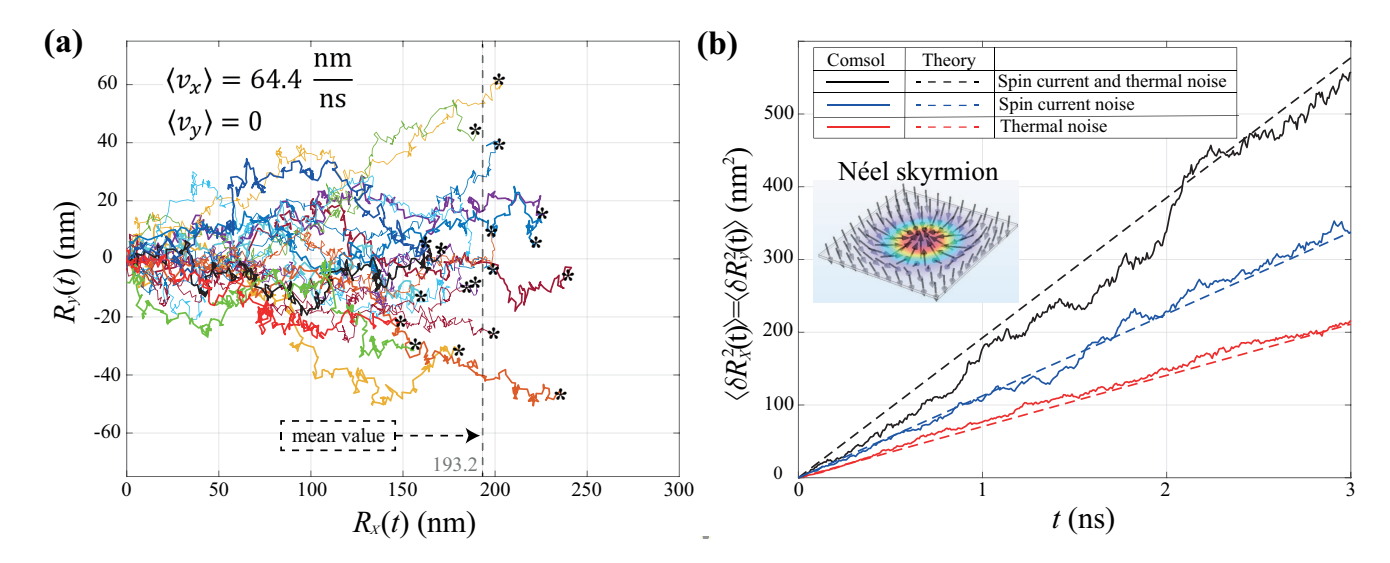


FIG. 1. (a) Example trajectories of Néel skyrmion motion under the combined influence of thermal and spin-current noise. The racetrack width of 150 nm is chosen to be sufficiently large to prevent skyrmion interaction with the racetrack boundaries during a 3 ns current pulse. (b) MSD of the skyrmion position obtained from both micromagnetic simulations (solid lines, 100 trajectories) and the analytical calculations (dashed lines). The results are shown for the cases with only thermal noise, only spin-current noise, and both noise sources (from bottom to top, respectively).

and $G_{xy} = G$ [54], which is also confirmed by our micromagnetic simulations. The solution of Eq. (5) for the velocity $\mathbf{v}(t) = \dot{\mathbf{R}}(t)$ of the skyrmion is given by

$$v_x = \frac{-GF_y - \alpha DF_x}{G^2 + \alpha^2 D^2}, \quad v_y = \frac{GF_x - \alpha DF_y}{G^2 + \alpha^2 D^2}.$$
 (8)

After evaluating the velocity correlation functions and integrating over time $\mathbf{R}(t) = \int_0^t \mathbf{v}(t')dt'$ (see details in the Supplemental Material, Section II) one obtains the MSD $\langle \delta \mathbf{R}^2(t) \rangle = \langle (\mathbf{R}(t) - \langle \mathbf{R}(t) \rangle)^2 \rangle$,

$$\langle \delta R_x^2(t) \rangle = \langle \delta R_y^2(t) \rangle = 2\mathcal{D}t,$$
 (9)

where the total diffusion coefficient $\mathcal{D} = \mathcal{D}_T + \mathcal{D}_I$ accounts for the respective contributions of thermal and spin current noise fluctuations,

$$\mathcal{D}_{T} = \frac{\alpha D}{2(G^{2} + \alpha^{2}D^{2})} 2k_{B}T,$$

$$\mathcal{D}_{I} = \frac{\alpha D(1 + \beta^{2})}{2(G^{2} + \alpha^{2}D^{2})} \frac{\delta \varepsilon}{E_{F}} (eU \coth \frac{eU}{2k_{B}T} - 2k_{B}T).$$
(10)

Note the non-monotonic dependence of the diffusion coefficient \mathcal{D} on the damping parameter α , which results in diffusion suppression as $\alpha \to 0$. This behavior is characteristic of skyrmions, in contrast to domain walls, for which G = 0, and $\mathcal{D} \sim 1/\alpha$ [54, 55].

Micromagnetic simulations were performed using the micromagnetic module of COMSOL Multiphysics [56, 57] for a two-dimensional system. A comparison between this module and mumax³ [58] is presented in the Supplemental Material, Section III. We extended the COMSOL module with a user-defined code that incorporates

thermal and spin-current fluctuations in accordance with Eqs. (4). The following parameters of the effective field $\mathbf{H}_{\mathrm{eff}}$ (see Supplemental Material, Section III) were used in the simulations: exchange coefficient $A_{\rm ex} = 10^{-11} \, {\rm J/m}$, anisotropy $K_u = 10^6 \text{ J/m}^3$, saturation magnetization $M_s = 0.6 \cdot 10^6$ A/m, interfacial DMI constant $D_{\rm DMI} =$ $-3.5 \cdot 10^{-3}$ J/m², and damping parameters $\alpha = \beta =$ 0.3. The racetrack sample has an (x-y) cross section of $500 \times 150 \text{ nm}^2$ and thickness $\Delta_f = 1 \text{ nm}$. The applied current density is $J = 4 \cdot 10^{11} \text{ A/m}^2$, the voltage is U = 0.5 V, and a linear current-voltage relationship $J \propto U$ is assumed. The temperature is set to T = 300 K. These parameters are typical of experimental racetrack systems [16, 45, 46]. The topological properties of skyrmions are fully characterized by three quantities (Q, Q_v, Q_h) , representing the topological charge, vorticity number, and helicity number, respectively [59, 60]. We restrict our analysis to the DMI, that stabilizes Néeltype skyrmions with $(1, 1, \pi)$.

Using micromagnetic modeling, the gyrocoupling constant G and dissipation tensor component D take the following values: $G = 4\pi M_s \Delta_f/\gamma$ and $D = 18.1 M_s \Delta_f/\gamma$ (see details in the Supplemental Material, Section III). In this work, we focus on the current-driven motion of skyrmions along the x-axis, which can be achieved by suppressing the transverse motion along the y-axis induced by the skyrmion Hall effect [61]. Following Ref. [62], the condition $\langle v_y \rangle = 0$ can be satisfied by choosing the angle ψ of the polarization vector \mathbf{p} as

$$\psi = \arctan \frac{G}{\alpha D} + \frac{\pi}{2} - Q_h. \tag{11}$$

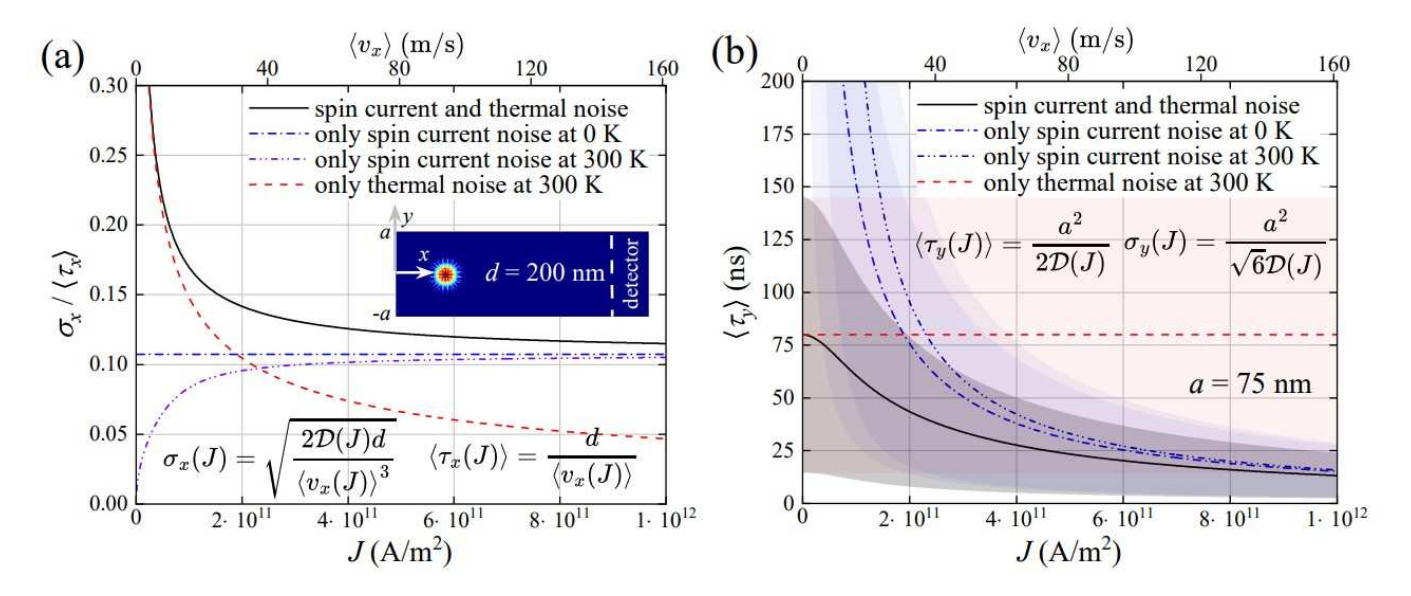


FIG. 2. (a) Normalized SD of the FPT to reach the detector position (x-direction), and (b) Mean FPT to reach the racetrack boundary $\pm a$ (y-direction) as functions of the current density J for various combinations of noises. Shaded regions in panel (b) indicate the standard deviations of the mean FPT along the y-axis. Here d=200 nm, a=75 cm.

For the Néel skyrmion, this yields $\psi = -23.36^{\circ}$, which is consistent with our micromagnetic simulations (note that the angle δ in Ref. [62] corresponds to ψ as $\delta = \psi - \pi/2$). For the chosen set of parameters the resulting drift velocity along the x-axis is estimated as $\langle v_x \rangle = 64.4$ m/s (see Supplemental Material, Section III).

Exemplary skyrmion trajectories obtained from micromagnetic simulations using COMSOL multiphysics are shown in Fig. 1(a), where both thermal and spin-current noises are taken into account. The current pulse duration is set to 3 ns, resulting in a mean displacement along the x-axis of 193.2 nm. The final skyrmion positions after 3 ns are marked by black asterisks. It can be seen that thermal and spin-current fluctuations cause significant random deviations around the mean position in both the x- and y-directions. The MSDs along both axes, obtained from simulated trajectories, are shown by solid lines in Fig. 1(b) together with the corresponding MSDs calculated from the Thiele approach, Eqs. (9, 10), shown by the dashed lines. The Figure demonstrates excellent agreement between the micromagnetic simulations and the analytical predictions based on the Thiele formalism. For the selected system parameters, nonequilibrium fluctuations dominate over equilibrium (thermal) fluctuations.

We now proceed to study the first passage problem for skyrmions on the racetrack in the situation where the skyrmion Hall effect and therefore the transverse drift across the racetrack, are absent. Using Eqs. (5)-(10) we rewrite the Thiele equation (5) in the form of a standard stochastic equation of motion

$$d\mathbf{R} = \langle \mathbf{v} \rangle dt + \boldsymbol{\xi} \sqrt{2\mathcal{D}dt}.$$
 (12)

Here, $\langle \mathbf{v} \rangle$ is the mean drift velocity, whose components are determined from Eq. (8), and $\boldsymbol{\xi} = (\xi_1, \xi_2)^T$ is a random vector with a normal distribution characterized by $\langle \xi_1 \rangle = \langle \xi_2 \rangle = 0$ and $\langle \xi_1 \xi_2 \rangle = 0$. This form is particularly convenient for analyzing first passage phenomena [63, 64]. Here, we focus on the mean FPTs $\langle \tau_{x,y} \rangle$ along and across the racetrack, as well as their SDs $\sigma_{x,y} = \sqrt{\langle \tau_{x,y}^2 \rangle - \langle \tau_{x,y} \rangle^2}$. The details of the FPT solutions for semi-infinite and finite domains are provided in the Supplemental Material, Section IV. Figure 2(a) illustrates the nontrivial behavior of the normalized SD $\sigma_x/\langle \tau_x \rangle = \sqrt{2\mathcal{D}(J)/(\langle v_x(J)\rangle d)}$ for the FPT along the racetrack as the function of the current density J, where d denotes the distance between the initial position at t=0 and the detector. For skyrmion diffusion across the racetrack, the mean FPT to reach the racetrack side boundaries $\pm a$ and its SD are given by $\langle \tau_y \rangle = a^2/(2\mathcal{D})$ and $\sigma_y = a^2/(\sqrt{6}\mathcal{D})$, respectively, differing only by a constant prefactor. Figure 2(b) presents the mean FPT $\langle \tau_u(J) \rangle$ across the racetrack with a=75 nm as a function of the current density J in the presence of thermal and/or spin current fluctuations.

The analytical results presented in Fig. 2(a) indicate that the spread of the mean FPT along the racetrack is governed by thermal fluctuations at low drift velocities, whereas at higher, yet still experimentally typical, velocities for present-day racetracks, non-equilibrium spin-current fluctuations become dominant. Remarkably, at zero temperature the normalized standard deviation of the FPT is independent of the current density. As the current density increases, the normalized total spread of the mean FPT approaches a constant value determined

by spin-current fluctuations at zero temperature.

Figure 2(b) shows the mean FPT across the racetrack as a function of the current density. Owing to the suppression of the skyrmion Hall effect, the motion along the y-axis is purely diffusive in nature. Similar to the motion along the racetrack, at low current densities (corresponding to low drift velocities) the mean FPT in the transverse direction is governed by thermal fluctuations, whereas at higher currents, spin-current fluctuations dominate the process of reaching the boundaries. For the parameters used here, the mean FPT along the y-axis exceeds the typical duration of the current-pulse sequence [46]; however, hitting the boundary can become significant for narrow racetracks due to the quadratic dependence on the racetrack width.

We developed an analytical framework to describe the combined effects of equilibrium (thermal) and nonequilibrium (spin-current) fluctuations on skyrmion dynamics in racetrack systems. Using the Thiele approach, we reduced the stochastic Landau–Lifshitz–Gilbert equation to a Langevin-like form for the skyrmion center of mass, allowing analytical evaluation of the mean squared displacement and first-passage time. The skyrmion exhibits normal diffusion with a coefficient governed by thermal fluctuations at low current densities, while spin-current noise dominates at higher, yet experimentally relevant, currents. Even in the absence of the skyrmion Hall effect, diffusive motion can drive the skyrmion to the racetrack boundaries, with the mean FPT across the track becoming comparable to the measurement time for low currents and narrow geometries. Micromagnetic simulations including both fluctuation sources confirm these analytical results.

Random displacements of magnetic textures represent a key source of bit-position and timing errors in high-speed racetrack memory devices [47, 65–67]. Beyond homogeneous systems, spatial disorder in the energy landscape [68, 69] arising from variations in magnetic anisotropy or DMI can induce pinning and anomalous diffusion [70–72]. Together with stochastic texture-creation errors [47], these effects call for extending the present theory to include diverse noise mechanisms that ultimately limit the reliability of racetrack operation.

Acknowledgments. The authors acknowledge illuminating discussions with S.S.P. Parkin and J.-C. Jeon, and financial support from the BMBF project 01DK24006 PLASMA-SPIN-ENERGY. AVH also acknowledges support of the STCU grant No. 9918 under the "2025 IEEE in Ukraine initiative".

- [2] S. Parkin and S.-H. Yang, Memory on the racetrack, Nat. Nanotechnol. 10, 195 (2015).
- [3] R. Bläsing, A. A. Khan, P. C. Filippou, C. Garg, F. Hameed, J. Castrillon, and S. S. Parkin, Magnetic racetrack memory: From physics to the cusp of applications within a decade, Proc. IEEE 108, 1303 (2020).
- [4] U. K. Rößler, A. Bogdanov, and C. Pfleiderer, Spontaneous skyrmion ground states in magnetic metals, Nature 442, 797 (2006).
- [5] S. Mühlbauer, B. Binz, F. Jonietz, C. Pfleiderer, A. Rosch, A. Neubauer, R. Georgii, and P. Böni, Skyrmion lattice in a chiral magnet, Science 323, 915 (2009).
- [6] S. X. Huang and C. L. Chien, Extended skyrmion phase in epitaxial FeGe(111) thin films, Phys. Rev. Lett. 108, 267201 (2012).
- [7] N. Nagaosa and Y. Tokura, Topological properties and dynamics of magnetic skyrmions, Nat. Nanotechnol. 8, 899 (2013).
- [8] L. Sun, R. X. Cao, B. F. Miao, Z. Feng, B. You, D. Wu, W. Zhang, A. Hu, and H. F. Ding, Creating an artificial two-dimensional skyrmion crystal by nanopatterning, Phys. Rev. Lett. 110, 167201 (2013).
- [9] P. Ferriani, K. von Bergmann, E. Y. Vedmedenko, S. Heinze, M. Bode, M. Heide, G. Bihlmayer, S. Blügel, and R. Wiesendanger, Atomic-scale spin spiral with a unique rotational sense: Mn monolayer on w(001), Phys. Rev. Lett. 101, 027201 (2008).
- [10] S. Heinze, K. von Bergmann, M. Menzel, J. Brede, A. Kubetzka, R. Wiesendanger, G. Bihlmayer, and S. Blügel, Spontaneous atomic-scale magnetic skyrmion lattice in two dimensions, Nature Physics 7, 713 (2011).
- [11] P. Wang, R. Saha, H. L. Meyerheim, K. Gu, H. Deniz, D. Eilmsteiner, A. Migliorini, J. R. Zuazo, E. Sebastiani-Tofano, I. Kostanovski, A. K. Srivastava, A. Ernst, and S. S. P. Parkin, High temperature neel skyrmions in simple ferromagnets (2025), arXiv:2510.06488 [cond-mat.mtrl-sci].
- [12] J. Slonczewski, Current-driven excitation of magnetic multilayers, J. Magn. Magn. Mater. 159, L1 (1996).
- [13] Z. Li and S. Zhang, Domain-wall dynamics and spin-wave excitations with spin-transfer torques, Phys. Rev. Lett. 92, 207203 (2004).
- [14] A. Thiaville, Y. Nakatani, J. Miltat, and Y. Suzuki, Micromagnetic understanding of current-driven domain wall motion in patterned nanowires, Europhys. Lett. 69, 990 (2005).
- [15] V. K. Dugaev, V. R. Vieira, P. D. Sacramento, J. Barnaś, M. A. N. Araújo, and J. Berakdar, Current-induced motion of a domain wall in a magnetic nanowire, Phys. Rev. B 74, 054403 (2006).
- [16] J. Sampaio, V. Cros, S. Rohart, A. Thiaville, and A. Fert, Nucleation, stability and current-induced motion of isolated magnetic skyrmions in nanostructures, Nature Nanotechnology 8, 839 (2013).
- [17] B. Dieny, I. L. Prejbeanu, K. Garello, P. Gambardella, P. Freitas, R. Lehndorff, W. Raberg, U. Ebels, S. O. Demokritov, J. Akerman, A. Deac, P. Pirro, C. Adelmann, A. Anane, A. V. Chumak, A. Hirohata, S. Mangin, S. O. Valenzuela, M. C. Onbasli, M. d'Aquino, G. Prenat, G. Finocchio, L. Lopez-Diaz, R. Chantrell, O. Chubykalo-Fesenko, and P. Bortolotti, Opportunities and challenges for spintronics in the microelectronics industry, Nat. Electron. 3, 446 (2020).

^{*} achechkin@mpi-halle.mpg.de

S. S. P. Parkin, M. Hayashi, and L. Thomas, Magnetic domain-wall racetrack memory, Science 320, 190 (2008).

- [18] J. E. Hirsch, Spin hall effect, Phys. Rev. Lett. 83, 1834 (1999).
- [19] I. Mihai Miron, G. Gaudin, S. Auffret, B. Rod-macq, A. Schuhl, S. Pizzini, J. Vogel, and P. Gambardella, Current-driven spin torque induced by the rashba effect in a ferromagnetic metal layer, Nature Materials 9, 230 (2010).
- [20] Q. Shao, P. Li, L. Liu, H. Yang, S. Fukami, A. Razavi, H. Wu, K. Wang, F. Freimuth, Y. Mokrousov, M. D. Stiles, S. Emori, A. Hoffmann, J. Åkerman, K. Roy, J.-P. Wang, S.-H. Yang, K. Garello, and W. Zhang, Roadmap of spin-orbit torques, IEEE Trans. Magn. 57, 1 (2021).
- [21] W. F. Brown, Thermal fluctuations of a single-domain particle, Phys. Rev. 130, 1677 (1963).
- [22] R. Kubo and N. Hashitsume, Brownian Motion of Spins, Prog. Theor. Phys. Suppl. 46, 210 (1970).
- [23] D. A. Garanin, Fokker-planck and landaulifshitz-bloch equations for classical ferromagnets, Phys. Rev. B 55, 3050 (1997).
- [24] J. L. García-Palacios and F. J. Lázaro, Langevindynamics study of the dynamical properties of small magnetic particles, Phys. Rev. B 58, 14937 (1998).
- [25] R. F. L. Evans, D. Hinzke, U. Atxitia, U. Nowak, R. W. Chantrell, and O. Chubykalo-Fesenko, Stochastic form of the landau-lifshitz-bloch equation, Phys. Rev. B 85, 014433 (2012).
- [26] L. Chotorlishvili, Z. Toklikishvili, V. K. Dugaev, J. Barnaś, S. Trimper, and J. Berakdar, Fokker-planck approach to the theory of the magnon-driven spin seebeck effect, Phys. Rev. B 88, 144429 (2013).
- [27] S. R. Etesami, L. Chotorlishvili, A. Sukhov, and J. Berakdar, Longitudinal spin current induced by a temperature gradient in a ferromagnetic insulator, Phys. Rev. B 90, 014410 (2014).
- [28] A. F. Schäffer, L. Rózsa, J. Berakdar, E. Y. Vedmedenko, and R. Wiesendanger, Stochastic dynamics and pattern formation of geometrically confined skyrmions, Commun. Phys. 2, 72 (2019).
- [29] M. Weißenhofer, L. Rózsa, and U. Nowak, Skyrmion dynamics at finite temperatures: Beyond thiele's equation, Phys. Rev. Lett. 127, 047203 (2021).
- [30] E. G. Mishchenko, Shot noise in a diffusive ferromagnetic-paramagnetic-ferromagnetic spin valve, Phys. Rev. B 68, 100409 (2003).
- [31] W. Belzig and M. Zareyan, Spin-flip noise in a multiterminal spin valve, Phys. Rev. B 69, 140407 (2004).
- [32] O. Sauret and D. Feinberg, Spin-current shot noise as a probe of interactions in mesoscopic systems, Phys. Rev. Lett. 92, 106601 (2004).
- [33] B. Wang, J. Wang, and H. Guo, Shot noise of spin current, Phys. Rev. B 69, 153301 (2004).
- [34] J. Foros, A. Brataas, Y. Tserkovnyak, and G. E. W. Bauer, Magnetization noise in magnetoelectronic nanostructures, Phys. Rev. Lett. 95, 016601 (2005).
- [35] R. L. Dragomirova and B. K. Nikolić, Shot noise of spin-polarized charge currents as a probe of spin coherence in spin-orbit coupled nanostructures, Phys. Rev. B 75, 085328 (2007).
- [36] A. L. Chudnovskiy, J. Swiebodzinski, and A. Kamenev, Spin-torque shot noise in magnetic tunnel junctions, Phys. Rev. Lett. 101, 066601 (2008).
- [37] J. Meair, P. Stano, and P. Jacquod, Measuring spin accumulations with current noise, Phys. Rev. B 84, 073302 (2011).

- [38] A. Chudnovskiy, C. Hübner, В. Baxevanis, and D. Pfannkuche, Spin switching: quasiclassical From quantum to approach, physica status solidi (b) **251**, 1764 (2014).
- [39] T. Szczepański, V. K. Dugaev, J. Barnaś, I. Martinez, J. P. Cascales, J.-Y. Hong, M.-T. Lin, and F. G. Aliev, Shot noise in magnetic tunneling structures with twolevel quantum dots, Phys. Rev. B 94, 235429 (2016).
- [40] A. Qaiumzadeh and A. Brataas, Quantum magnetization fluctuations via spin shot noise, Phys. Rev. B 98, 220408 (2018).
- [41] S. Woo, K. Litzius, B. Krüger, M.-Y. Im, L. Caretta, K. Richter, M. Mann, A. Krone, R. M. Reeve, M. Weigand, P. Agrawal, I. Lemesh, M.-A. Mawass, P. Fischer, M. Kläui, and G. S. D. Beach, Observation of room-temperature magnetic skyrmions and their current-driven dynamics in ultrathin metallic ferromagnets, Nat. Mater. 15, 501 (2016).
- [42] E. Y. Vedmedenko, R. K. Kawakami, D. D. Sheka, P. Gambardella, A. Kirilyuk, A. Hirohata, C. Binek, O. Chubykalo-Fesenko, S. Sanvito, B. J. Kirby, J. Grollier, K. Everschor-Sitte, T. Kampfrath, C.-Y. You, and A. Berger, The 2020 magnetism roadmap, J. Phys. D: Appl. Phys. 53, 453001 (2020).
- [43] T. da Câmara Santa Clara Gomes, Y. Sassi, D. Sanz-Hernández, S. Krishnia, S. Collin, M.-B. Martin, P. Seneor, V. Cros, J. Grollier, and N. Reyren, Neuromorphic weighted sums with magnetic skyrmions, Nat. Electron. 8, 204 (2025).
- [44] A. Zholud, R. Freeman, R. Cao, A. Srivastava, and S. Urazhdin, Spin transfer due to quantum magnetization fluctuations, Phys. Rev. Lett. 119, 257201 (2017).
- [45] J.-C. Jeon, A. Migliorini, L. Fischer, J. Yoon, and S. S. P. Parkin, Dynamic manipulation of chiral domain wall spacing for advanced spintronic memory and logic devices, ACS Nano 18, 14507 (2024).
- [46] J.-C. Jeon, A. Migliorini, J. Yoon, J. Jeong, and S. S. P. Parkin, Multicore memristor from electrically readable nanoscopic racetracks, Science 386, 315 (2024).
- [47] M. Ishibashi, M. Kawaguchi, Y. Hibino, K. Yakushiji, A. Tsukamoto, S. Nakatsuji, and M. Hayashi, Decoding the magnetic bit positioning error in a ferrimagnetic racetrack, Science Advances 10, eadq0898 (2024).
- [48] W. Jiang, X. Zhang, G. Yu, W. Zhang, X. Wang, M. Benjamin Jungfleisch, J. E. Pearson, X. Cheng, O. Heinonen, K. L. Wang, Y. Zhou, A. Hoffmann, and S. G. E. te Velthuis, Direct observation of the skyrmion hall effect, Nature Physics 13, 162 (2017).
- [49] L. D. Landau and E. Lifshitz, On the theory of the dispersion of magnetic permeability in ferromagnetic bodies, Phys. Z. Sowjet. 8, 153 (1935).
- [50] T. Gilbert, A phenomenological theory of damping in ferromagnetic materials, IEEE Trans. Magn. 40, 3443 (2004).
- [51] Y. Blanter and M. Büttiker, Shot noise in mesoscopic conductors, Physics Reports 336, 1 (2000).
- [52] A. A. Thiele, Steady-state motion of magnetic domains, Phys. Rev. Lett. 30, 230 (1973).
- [53] T. Kamppeter, F. G. Mertens, E. Moro, A. Sánchez, and A. R. Bishop, Stochastic vortex dynamics in twodimensional easy-plane ferromagnets: Multiplicative versus additive noise, Phys. Rev. B 59, 11349 (1999).
- [54] J. Miltat, S. Rohart, and A. Thiaville, Brownian motion of magnetic domain walls and skyrmions, and their dif-

- fusion constants, Phys. Rev. B 97, 214426 (2018).
- [55] C. Schütte, J. Iwasaki, A. Rosch, and N. Nagaosa, Inertia, diffusion, and dynamics of a driven skyrmion, Phys. Rev. B 90, 174434 (2014).
- [56] W. Yu, Micromagnetics module for comsol multiphysics, https://www.comsol.com/community/exchange/883/, version 2.13, Accessed: 2025-09-15.
- [57] W. Yu, Micromagnetics Module User's Guide (V1.33), Fudan University (2020), accessed: 2025-09-15.
- [58] A. Vansteenkiste, J. Leliaert, M. Dvornik, M. Helsen, F. Garcia-Sanchez, and B. Van Waeyenberge, The design and verification of mumax3, AIP Adv. 4, 107133 (2014).
- [59] I. A. Ado, O. A. Tretiakov, and M. Titov, Microscopic theory of spin-orbit torques in two dimensions, Phys. Rev. B 95, 094401 (2017).
- [60] X. Zhang, Y. Zhou, K. Mee Song, T.-E. Park, J. Xia, M. Ezawa, X. Liu, W. Zhao, G. Zhao, and S. Woo, Skyrmion-electronics: writing, deleting, reading and processing magnetic skyrmions toward spintronic applications, J. Phys.: Condens. Matter 32, 143001 (2020).
- [61] W. Jiang, X. Zhang, G. Yu, W. Zhang, X. Wang, M. Benjamin Jungfleisch, J. E. Pearson, X. Cheng, O. Heinonen, K. L. Wang, Y. Zhou, A. Hoffmann, and S. G. te Velthuis, Direct observation of the skyrmion hall effect, Nat. Phys. 13, 162 (2017).
- [62] B. Göbel, A. Mook, J. Henk, and I. Mertig, Overcoming the speed limit in skyrmion racetrack devices by suppressing the skyrmion hall effect, Phys. Rev. B 99, 020405 (2019).
- [63] D. R. Cox and H. D. Miller, Theory of Stochastic Processes (Chapman & Hall/CRC, 2001).
- [64] S. Redner, A Guide to First-Passage Processes (Cambridge University Press, 2001).
- [65] Z. Sun, W. Wu, and H. Li, Cross-layer racetrack memory

- design for ultra high density and low power consumption, in 2013 50th ACM/EDAC/IEEE Design Automation Conference (DAC) (2013) pp. 1–6.
- [66] C. Zhang, G. Sun, X. Zhang, W. Zhang, W. Zhao, T. Wang, Y. Liang, Y. Liu, Y. Wang, and J. Shu, Hi-fi playback: tolerating position errors in shift operations of racetrack memory, SIGARCH Comput. Archit. News 43, 694-706 (2015).
- [67] Y. M. Chee, H. M. Kiah, A. Vardy, V. K. Vu, and E. Yaakobi, Coding for racetrack memories, IEEE Transactions on Information Theory 64, 7094 (2018).
- [68] X. Jiang, L. Thomas, R. Moriya, M. Hayashi, B. Bergman, C. Rettner, and S. S. Parkin, Enhanced stochasticity of domain wall motion in magnetic racetracks due to dynamic pinning, Nat. Commun. 1, 25 (2010).
- [69] H.-S. Lee, K.-S. Ryu, C.-Y. You, K.-R. Jeon, S. S. P. Parkin, and S.-C. Shin, Reduced stochasticity in domain wall motion with increasing pinning density in thin fe films, New J. Phys. 13, 083038 (2011).
- [70] D. Ravelosona, S. Mangin, J. A. Katine, E. E. Fullerton, and B. D. Terris, Threshold currents to move domain walls in films with perpendicular anisotropy, Appl. Phys. Lett. 90, 072508 (2007).
- [71] T. Herranen and L. Laurson, Barkhausen noise from precessional domain wall motion, Phys. Rev. Lett. 122, 117205 (2019).
- [72] M. Kawaguchi, K. Tanabe, K. Yamada, T. Sawa, S. Hasegawa, M. Hayashi, and Y. Nakatani, Determination of the dzyaloshinskii-moriya interaction using pattern recognition and machine learning, npj Comput. Mater. 7, 20 (2021).

SUPPLEMENTARY MATERIAL

This supplementary information provides a detailed derivation and study of: I) the derivation of the Thiele equations; II) the derivation of fluctuation forces and diffusion coefficients of magnetic textures; III) the details of the micromagnetic simulations; IV) the derivation of the first-passage-time moments of the stochastic equations.

I. THE THIELE EQUATION

The stochastic LLG equation is:

$$\partial_t \mathbf{M} + \gamma \mathbf{M} \times (\mathbf{H}_{\text{eff}} + \delta \mathbf{h}) - \frac{\alpha}{M_s} \mathbf{M} \times \partial_t \mathbf{M} + \frac{\gamma}{M_s^2 \mathcal{V}} \mathbf{M} \times (\mathbf{M} \times (\mathbf{I}_s + \delta \mathbf{I})) + \frac{\gamma \beta}{M_s \mathcal{V}} \mathbf{M} \times (\mathbf{I}_s + \delta \mathbf{I}) = 0.$$
 (13)

To further study the dynamics of magnetic textures, we turn to the Thiele approach (first proposed for magnetic domains [52]), which involves considering the traveling-wave Ansatz $\mathbf{M} = \mathbf{M}(\mathbf{r} - \mathbf{R}(t))$ and results in $\partial_t \mathbf{M}(\mathbf{r} - \mathbf{R}(t)) = -\nabla_i \mathbf{M} \ R_i(t)$. In our study, we omit the higher derivatives of $\mathbf{R}(t)$ [53], which affect a small initial time interval (characteristic time amounts to several tens of picoseconds [54]). To obtain the Thiele stochastic equation, we begin with Eq. 13 and multiply it by $\frac{1}{M_s^2 \gamma} \mathbf{M} \cdot [\nabla_i \mathbf{M} \times \ldots]$, followed by integration over \mathbf{r} . We also use the following relations: $M_i \cdot M_i = M_s^2$, $\nabla_j M_i \cdot M_i = 0$, and $\partial_t M_i \cdot M_i = 0$ [52]. Each term in Eq. 13 generates a separate force.

• The gyrotropic force have the following form:

$$\frac{1}{M_s^2 \gamma} \int \mathbf{M} \cdot [\nabla_i \mathbf{M} \times \partial_t \mathbf{M}] d\mathbf{r} = \frac{-1}{M_s^2 \gamma} \int \mathbf{M} \cdot [\nabla_i \mathbf{M} \times \nabla_j \mathbf{M}] d\mathbf{r} \cdot \dot{R}_j = \hat{G} \cdot \dot{\mathbf{R}}, G_{ij} = \frac{-1}{M_s^2 \gamma} \int \mathbf{M} \cdot [\nabla_i \mathbf{M} \times \nabla_j \mathbf{M}] d\mathbf{r}. \quad (14)$$

• The force generated by the effective field:

$$\frac{1}{M_s^2} \int \mathbf{M} \cdot [\nabla_i \mathbf{M} \times [\mathbf{M} \times \mathbf{H}_{\text{eff}}]] d\mathbf{r} = \frac{1}{M_s^2} \int \mathbf{M} \cdot [\mathbf{M}(\nabla_i \mathbf{M} \cdot \mathbf{H}_{\text{eff}}) - \mathbf{H}_{\text{eff}}(\nabla_i \mathbf{M} \cdot \mathbf{M})] d\mathbf{r} = \int \nabla_i \mathbf{M} \cdot \mathbf{H}_{\text{eff}} d\mathbf{r}.$$
(15)

• The thermal fluctuation force:

$$\frac{1}{M_s^2} \int \mathbf{M} \cdot [\nabla_i \mathbf{M} \times [\mathbf{M} \times \delta \mathbf{h}]] d\mathbf{r} = \frac{1}{M_s^2} \int \mathbf{M} \cdot [\mathbf{M} (\nabla_i \mathbf{M} \cdot \delta \mathbf{h}) - \delta \mathbf{h} (\nabla_i \mathbf{M} \cdot \mathbf{M})] d\mathbf{r} = \int \nabla_i \mathbf{M} \cdot \delta \mathbf{h} d\mathbf{r}.$$
(16)

• The dissipation force:

$$\frac{-\alpha}{M_s^3 \gamma} \int \mathbf{M} \cdot [\nabla_i \mathbf{M} \times [\mathbf{M} \times \partial_t \mathbf{M}]] d\mathbf{r} = \frac{-\alpha}{M_s^3 \gamma} \int \mathbf{M} \cdot [\mathbf{M}(\nabla_i \mathbf{M} \cdot \partial_t \mathbf{M}) - \partial_t \mathbf{M}(\nabla_i \mathbf{M} \cdot \underline{\mathbf{M}})] d\mathbf{r}$$

$$= \frac{-\alpha}{M_s^3 \gamma} \int M_s^2 (\nabla_i \mathbf{M} \cdot \partial_t \mathbf{M}) d\mathbf{r} = \frac{\alpha}{M_s \gamma} \int \nabla_i \mathbf{M} \cdot \nabla_j \mathbf{M} d\mathbf{r} \dot{R}_j = \alpha \hat{D} \cdot \dot{\mathbf{R}}, D_{ij} = \frac{1}{M_s \gamma} \int \nabla_i \mathbf{M} \cdot \nabla_j \mathbf{M} d\mathbf{r}. \tag{17}$$

• Force induced by Slonczewski's torque term:

$$\frac{1}{M_s^4 \mathcal{V}} \int \mathbf{M} \cdot (\nabla_i \mathbf{M} \times [\mathbf{M} \times [\mathbf{M} \times \mathbf{I}_s]]) d\mathbf{r} = \frac{1}{M_s^4 \mathcal{V}} \int \mathbf{M} \cdot [\mathbf{M}(\nabla_i \mathbf{M} \cdot [\mathbf{M} \times \mathbf{I}_s]) - [\mathbf{M} \times \mathbf{I}_s](\nabla_i \mathbf{M} \cdot \mathbf{M})] d\mathbf{r}$$

$$= \frac{1}{M_s^2 \mathcal{V}} \int \nabla_i \mathbf{M} \cdot [\mathbf{M} \times \mathbf{I}_s] d\mathbf{r} = \frac{1}{M_s^2 \mathcal{V}} \int [\nabla_i \mathbf{M} \times \mathbf{M}] \cdot \mathbf{I}_s d\mathbf{r}. \tag{18}$$

• The damping-like torque force:

$$\frac{\beta}{M_s^3 \mathcal{V}} \int \mathbf{M} \cdot [\nabla_i \mathbf{M} \times [\mathbf{M} \times \mathbf{I}_s]] d\mathbf{r} = \frac{\beta}{M_s^3 \mathcal{V}} \int \mathbf{M} \cdot [\mathbf{M}(\nabla_i \mathbf{M} \cdot \mathbf{I}_s) - \mathbf{I}_s(\nabla_i \mathbf{M} \cdot \mathbf{M})] d\mathbf{r} = \frac{\beta}{M_s \mathcal{V}} \int \nabla_i \mathbf{M} \cdot \mathbf{I}_s d\mathbf{r}.$$
(19)

• The spin current fluctuation force:

$$\frac{1}{M_s^4 \mathcal{V}} \int \mathbf{M} \cdot (\nabla_i \mathbf{M} \times [\mathbf{M} \times [\mathbf{M} \times \delta \mathbf{I}]]) d\mathbf{r} + \frac{\beta}{M_s^3 \mathcal{V}} \int \mathbf{M} \cdot [\nabla_i \mathbf{M} \times [\mathbf{M} \times \delta \mathbf{I}]] d\mathbf{r}$$

$$= \frac{1}{M_s^4 \mathcal{V}} \int \mathbf{M} \cdot [\mathbf{M} (\nabla_i \mathbf{M} \cdot [\mathbf{M} \times \delta \mathbf{I}]) - [\mathbf{M} \times \delta \mathbf{I}] (\nabla_i \mathbf{M} \cdot \mathbf{M})] d\mathbf{r} + \frac{\beta}{M_s^3 \mathcal{V}} \int \mathbf{M} \cdot [\mathbf{M} (\nabla_i \mathbf{M} \cdot \delta \mathbf{I}) - \delta \mathbf{I} (\nabla_i \mathbf{M} \cdot \mathbf{M})] d\mathbf{r} \quad (20)$$

$$= \frac{1}{M_s^2 \mathcal{V}} \int \nabla_i \mathbf{M} \cdot [\mathbf{M} \times \delta \mathbf{I}] d\mathbf{r} + \frac{\beta}{M_s \mathcal{V}} \int \nabla_i \mathbf{M} \cdot \delta \mathbf{I} d\mathbf{r} = \frac{1}{M_s^2 \mathcal{V}} \int [\nabla_i \mathbf{M} \times \mathbf{M}] \cdot \delta \mathbf{I} d\mathbf{r} + \frac{\beta}{M_s \mathcal{V}} \int \nabla_i \mathbf{M} \cdot \delta \mathbf{I} d\mathbf{r}.$$

Using equations 14-20 we can rewrite LLG equation 13 in the form of the so-called the Thiele equation:

$$\widehat{G} \cdot \dot{\mathbf{R}} + \alpha \widehat{D} \cdot \dot{\mathbf{R}} + \mathbf{F}_{eff} + \mathbf{F}_{SOT} + \mathbf{F}_{\delta h} + \mathbf{F}_{\delta I} = 0,
G_{ij} = -\frac{1}{M_s^2 \gamma} \int \mathbf{M} \cdot [\nabla_i \mathbf{M} \times \nabla_j \mathbf{M}] d\mathbf{r}, \quad \frac{[\mathbf{A} \, \mathbf{m}^{-1} \cdot \mathbf{m}^{-1} \cdot \mathbf{A} \, \mathbf{m}^{-1} \cdot \mathbf{m}^{-1} \cdot \mathbf{A} \, \mathbf{m}^{-1} \cdot \mathbf{m}^{3}]}{[\mathbf{A}^{2} \, \mathbf{m}^{-2} \cdot \mathbf{A} \, \mathbf{s} \, \mathbf{kg}^{-1}]} = [\mathbf{kg} \, \mathbf{s}^{-1}],
D_{ij} = \frac{1}{M_s \gamma} \int \nabla_i \mathbf{M} \cdot \nabla_j \mathbf{M} d\mathbf{r}, \quad \frac{[\mathbf{m}^{-1} \cdot \mathbf{A} \, \mathbf{m}^{-1} \cdot \mathbf{m}^{-1} \cdot \mathbf{A} \, \mathbf{m}^{-1} \cdot \mathbf{m}^{3}]}{[\mathbf{A} \, \mathbf{m}^{-1} \cdot \mathbf{A} \, \mathbf{s} \, \mathbf{kg}^{-1}]} = [\mathbf{kg} \, \mathbf{s}^{-1}],
\mathbf{F}_{eff} = \int \nabla_i \mathbf{M} \cdot \mathbf{H}_{eff} d\mathbf{r}, \quad [\mathbf{m}^{-1} \cdot \mathbf{A} \, \mathbf{m}^{-1} \cdot \mathbf{T} \cdot \mathbf{m}^{3}] = [\mathbf{m}^{-1} \cdot \mathbf{A} \, \mathbf{m}^{-1} \cdot \mathbf{kg} \, \mathbf{s}^{-2} \mathbf{A}^{-1} \cdot \mathbf{m}^{3}] = [\mathbf{N}],
\mathbf{F}_{SOT} = \frac{1}{M_s^2 \mathcal{V}} \int [\nabla_i \mathbf{M} \times \mathbf{M}] \cdot \mathbf{I}_s d\mathbf{r} + \frac{\beta}{M_s \mathcal{V}} \int \nabla_i \mathbf{M} \cdot \mathbf{I}_s d\mathbf{r},
[\mathbf{m}^{-1} \cdot \mathbf{A} \, \mathbf{m}^{-1} \cdot \mathbf{A} \, \mathbf{m}^{-1} \cdot \mathbf{J} \cdot \mathbf{m}^{3}] + \frac{[\mathbf{m}^{-1} \cdot \mathbf{A} \, \mathbf{m}^{-1} \cdot \mathbf{J} \cdot \mathbf{m}^{3}]}{[\mathbf{A}^{2} \mathbf{m}^{-2} \cdot \mathbf{m}^{3}]} = [\mathbf{N}],
\mathbf{F}_{\delta h} = \int \nabla_i \mathbf{M} \cdot \delta \mathbf{h} d\mathbf{r}, \quad [\mathbf{m}^{-1} \cdot \mathbf{A} \, \mathbf{m}^{-1} \cdot \mathbf{T} \cdot \mathbf{m}^{3}] = [\mathbf{m}^{-1} \cdot \mathbf{A} \, \mathbf{m}^{-1} \cdot \mathbf{kg} \, \mathbf{s}^{-2} \mathbf{A}^{-1} \cdot \mathbf{m}^{3}] = [\mathbf{N}],
\mathbf{F}_{\delta I} = \frac{1}{M_s^2 \mathcal{V}} \int [\nabla_i \mathbf{M} \times \mathbf{M}] \cdot \delta \mathbf{I} d\mathbf{r} + \frac{\beta}{M_s \mathcal{V}} \int \nabla_i \mathbf{M} \cdot \delta \mathbf{I} d\mathbf{r},
[\mathbf{M}^{-1} \cdot \mathbf{A} \, \mathbf{m}^{-1} \cdot \mathbf{A} \, \mathbf{m}^{-1} \cdot \mathbf{J} \cdot \mathbf{m}^{3}] + \frac{[\mathbf{m}^{-1} \cdot \mathbf{A} \, \mathbf{m}^{-1} \cdot \mathbf{J} \cdot \mathbf{m}^{3}]}{[\mathbf{A}^{2} \mathbf{m}^{-2} \cdot \mathbf{m}^{3}]} = [\mathbf{N}].$$

Here and below, the dimensions of the corresponding quantities are indicated in square brackets.

The basic assumption of Thiele's approach is that the shape of the magnetic texture remains largely unchanged under the influence of perturbations, and only its position changes.

II. FLUCTUATION FORCES. DIFFUSION COEFFICIENTS OF MAGNETIC TEXTURES

The Thiele equations 21 contain two fluctuation forces of different nature: the first $\mathbf{F}_{\delta h}$ is caused by thermal fluctuations $\delta \mathbf{h}$, and the second $\mathbf{F}_{\delta I}$ by spin current fluctuations $\delta \mathbf{I}$. The correlation dependences of the indicated forces are derived from the known relationships for fluctuation fields $\delta \mathbf{h}$ and $\delta \mathbf{I}$:

$$\langle \delta h_i(t, \mathbf{r}) \delta h_j(t', \mathbf{r}') \rangle = 2 \mathcal{D}_T \delta_{ij} \delta(\mathbf{r} - \mathbf{r}') \delta(t - t') = \frac{2 \alpha k_B T}{\gamma M_s} \delta_{ij} \delta(\mathbf{r} - \mathbf{r}') \delta(t - t'), \frac{[\mathbf{J} \mathbf{K}^{-1} \cdot \mathbf{K} \cdot \mathbf{m}^{-3} \cdot s^{-1}]}{[\mathbf{A} \mathbf{s} \mathbf{kg}^{-1} \cdot \mathbf{A} \mathbf{m}^{-1}]} = [\mathbf{T}^2]$$

$$\langle \delta I_i(t, \mathbf{r}) \delta I_j(t', \mathbf{r}') \rangle = 2 \mathcal{D}_I \delta_{ij} \delta(\mathbf{r} - \mathbf{r}') \delta(t - t') = \frac{\alpha M_s \mathcal{V}^2}{\gamma} \frac{\delta \varepsilon}{E_F} (eU \coth \frac{eU}{2k_B T} - 2k_B T) \delta_{ij} \delta(\mathbf{r} - \mathbf{r}') \delta(t - t'), [\mathbf{J}^2]$$

$$\langle \delta h_i(t, \mathbf{r}) \delta I_j(t', \mathbf{r}') \rangle = 0.$$
(22)

First, we derive the autocorrelation for the force $F_{\delta h,i}$ that is caused by thermal fluctuations (following the approach from [53, 54])).

$$\langle F_{\delta h,i}F_{\delta h,j}\rangle = \left\langle \int \nabla_i M_m \delta h_m d\mathbf{r} \int \nabla_j M_n \delta h_n d\mathbf{r'} \right\rangle = \int \int \nabla_i M_m \nabla_j M_n \left\langle \delta h_m \delta h_n \right\rangle d\mathbf{r} d\mathbf{r'}$$

$$= 2\mathcal{D}_T \delta_{mn} \delta(t - t') \int \nabla_i M_m \nabla_j M_n d\mathbf{r} = 2\alpha k_B T D_{ij} \delta(t - t').$$
(23)

The thermal and spin-current noises we introduced are generally multiplicative; however, removing the magnetization vector gradient from the averaging brackets is justified by the assumption that this vector does not undergo strong perturbations relative to the noise-free case [53, 54]. Autocorrelation for force $F_{\delta I,i}$ is:

$$\langle F_{\delta I,i}F_{\delta I,j}\rangle = \frac{\beta^{2}}{M_{s}^{2}\mathcal{V}^{2}} \left\langle \int \nabla_{i}M_{m} \cdot \delta I_{m}d\mathbf{r} \int \nabla_{j}M_{n} \cdot \delta I_{n}d\mathbf{r}' \right\rangle + \frac{2\beta}{M_{s}^{2}\mathcal{V}^{2}} \left\langle \int \nabla_{i}M_{m} \cdot \delta I_{m}d\mathbf{r} \int [\nabla_{j}\mathbf{M} \times \mathbf{M}]_{n} \delta I_{n}d\mathbf{r}' \right\rangle + \frac{1}{M_{s}^{4}\mathcal{V}^{2}} \left\langle \int [\nabla_{i}\mathbf{M} \times \mathbf{M}]_{m} \cdot \delta I_{m}d\mathbf{r} \int [\nabla_{j}\mathbf{M} \times \mathbf{M}]_{n} \delta I_{n}d\mathbf{r}' \right\rangle = \frac{\beta^{2}}{M_{s}^{2}\mathcal{V}^{2}} \int \int \nabla_{i}M_{m} \cdot \nabla_{j}M_{n} \left\langle \delta I_{m}\delta I_{n} \right\rangle d\mathbf{r}d\mathbf{r}' + \frac{2\beta}{M_{s}^{2}\mathcal{V}^{2}} \int \int \nabla_{i}\mathbf{M} \times \mathbf{M} \int_{n} \left\langle \delta I_{m}\delta I_{n} \right\rangle d\mathbf{r}d\mathbf{r}' + \frac{1}{M_{s}^{4}\mathcal{V}^{2}} \int \int [\nabla_{i}\mathbf{M} \times \mathbf{M}]_{m} [\nabla_{j}\mathbf{M} \times \mathbf{M}]_{n} \left\langle \delta I_{m}\delta I_{n} \right\rangle d\mathbf{r}d\mathbf{r}' + \frac{2\mathcal{D}_{1}\beta^{2}\delta_{mn}\delta(t-t')}{M_{s}^{2}\mathcal{V}^{2}} \int \nabla_{i}\mathbf{M} \times \mathbf{M} \int_{n} \left\langle \delta I_{m}\delta I_{n} \right\rangle d\mathbf{r}d\mathbf{r}' + \frac{2\mathcal{D}_{1}\beta^{2}\delta_{mn}\delta(t-t')}{M_{s}^{2}\mathcal{V}^{2}} \int \nabla_{i}M_{m} \cdot \nabla_{j}M_{n}d\mathbf{r}$$

$$= \frac{2\mathcal{D}_{1}\delta(t-t')}{M_{s}^{4}\mathcal{V}^{2}} \int \nabla_{i}\mathbf{M} \cdot (\nabla_{j}\mathbf{M}M_{s}^{2} - \mathbf{M}(\nabla_{j}\mathbf{M} \cdot \mathbf{M}))d\mathbf{r} + \frac{2\mathcal{D}_{1}\beta^{2}\delta(t-t')}{M_{s}^{2}\mathcal{V}^{2}} \int \nabla_{i}\mathbf{M} \cdot \nabla_{j}\mathbf{M}d\mathbf{r}$$

$$= \frac{2\mathcal{D}_{1}(1+\beta^{2})\delta(t-t')}{M_{s}^{2}\mathcal{V}^{2}} \int \nabla_{i}\mathbf{M} \cdot \nabla_{j}\mathbf{M}d\mathbf{r} = \alpha(1+\beta^{2})\frac{\delta\varepsilon}{E_{F}} (eU \coth \frac{eU}{2k_{B}T} - 2k_{B}T)D_{ij}\delta(t-t')$$

$$(24)$$

It is easy to see that cross-correlations with thermal and spin current fluctuation forces are zero $\langle F_{\delta h,i}F_{\delta I_s,j}\rangle=0$. Below are the correlations for equilibrium and nonequilibrium stochastic forces:

$$\langle F_{\delta h,i} F_{\delta h,j} \rangle = 2\alpha k_B T D_{ij} \delta(t - t'),$$

$$\langle F_{\delta I,i} F_{\delta I,j} \rangle = \alpha (1 + \beta^2) \frac{\delta \varepsilon}{E_F} (eU \coth \frac{eU}{2k_B T} - 2k_B T) D_{ij} \delta(t - t'),$$

$$\langle F_{\delta I,i} F_{\delta h,j} \rangle = 0$$
(25)

In the case of two-dimensional structures such as magnetic films, we can rewrite system of equations 21 as:

$$-G_{xy}\dot{R}_{y} + \alpha D_{xx}\dot{R}_{x} + \alpha D_{xy}\dot{R}_{y} + F_{x} = 0,$$

$$G_{xy}\dot{R}_{x} + \alpha D_{xy}\dot{R}_{x} + \alpha D_{yy}\dot{R}_{y} + F_{y} = 0,$$
(26)

Here $\mathbf{F} = \mathbf{F}_{eff} + \mathbf{F}_{SOT} + \mathbf{F}_{\delta h} + \mathbf{F}_{\delta I}$. Next, solving linear algebraic equations 26, we find velocity $\mathbf{v} = \dot{\mathbf{R}}$.

$$\dot{R}_{x} = v_{x} = \frac{-G_{xy}F_{y} + \alpha D_{xy}F_{y} - \alpha D_{yy}F_{x}}{-\alpha^{2}D_{xy}^{2} + G_{xy}^{2} + \alpha^{2}D_{xx}D_{yy}},
\dot{R}_{y} = v_{y} = \frac{G_{xy}F_{x} + \alpha D_{xy}F_{x} - \alpha D_{xx}F_{y}}{-\alpha^{2}D_{xy}^{2} + G_{xy}^{2} + \alpha^{2}D_{xx}D_{yy}}.$$
(27)

Skirmion diffusion constant

The resulting Eqs. 25 and 26 make it possible to describe the diffusion of magnetic textures in thin ferromagnetic films. In the case of two-dimensional magnetic structures such as magnetic skyrmions, and following approach in [54], we can assume that $D_{xy} = 0$, $D_{xx} = D_{yy} = D$ and $G_{xy} = G$, which is also confirmed by our micromagnetic simulation. Next, we calculate the solution for the velocity $\dot{\mathbf{R}}(t) = v(t)$ of the skyrmion:

$$v_x = \frac{-GF_y - \alpha DF_x}{G^2 + \alpha^2 D^2},$$

$$v_y = \frac{GF_x - \alpha DF_y}{G^2 + \alpha^2 D^2}.$$
(28)

Next, we calculate the correlation relations for the components of the skyrmion velocity:

$$\langle v_x(t)v_x(t')\rangle = \frac{\langle -GF_y(t) - \alpha DF_x(t), -GF_y(t') - \alpha DF_x(t')\rangle}{(G^2 + \alpha^2 D^2)^2} = \frac{G^2\langle F_y(t)F_y(t')\rangle + \alpha^2 D^2\langle F_x(t)F_x(t')\rangle}{(G^2 + \alpha^2 D^2)^2}$$

$$= \frac{G^2(\langle F_{h,y}(t)F_{h,y}(t')\rangle + \langle F_{I,y}(t)F_{I,y}(t')\rangle) + \alpha^2 D^2(\langle F_{h,x}(t)F_{h,x}(t')\rangle + \langle F_{I,x}(t)F_{I,x}(t')\rangle)}{(G^2 + \alpha^2 D^2)^2}$$

$$= \frac{G^2(\langle F_{h,y}(t)F_{h,y}(t')\rangle + \langle F_{I,y}(t)F_{I,y}(t')\rangle) + \alpha^2 D^2(\langle F_{h,x}(t)F_{h,x}(t')\rangle + \langle F_{I,x}(t)F_{I,x}(t')\rangle)}{(G^2 + \alpha^2 D^2)^2}$$

$$= \frac{(G^2 + \alpha^2 D^2)(2k_B T + (1 + \beta^2)\frac{\delta \varepsilon}{E_F}(eV \cot \frac{eV}{2k_B T} - 2k_B T))\delta(t - t')}{G^2 + \alpha^2 D^2} ,$$

$$\langle v_y(t)v_y(t')\rangle = \frac{\langle GF_x(t) - \alpha DF_y(t), GF_x(t') - \alpha DF_y(t')\rangle}{(G^2 + \alpha^2 D^2)^2} = \frac{G^2\langle F_x(t)F_x(t')\rangle + \alpha^2 D^2\langle F_y(t)F_y(t')\rangle}{(G^2 + \alpha^2 D^2)^2}$$

$$= \frac{G^2(\langle F_{h,x}(t)F_{h,x}(t')\rangle + \langle F_{I,x}(t)F_{I,x}(t')\rangle) + \alpha^2 D^2(\langle F_{h,y}(t)F_{h,y}(t')\rangle + \langle F_{I,y}(t)F_{I,y}(t')\rangle)}{(G^2 + \alpha^2 D^2)^2}$$

$$= \frac{G^2(\langle F_{h,x}(t)F_{h,x}(t')\rangle + \langle F_{I,x}(t)F_{I,x}(t')\rangle) + \alpha^2 D^2(\langle F_{h,y}(t)F_{h,y}(t')\rangle + \langle F_{I,y}(t)F_{I,y}(t')\rangle)}{(G^2 + \alpha^2 D^2)^2}$$

$$= \frac{G^2(\langle F_{h,x}(t)F_{h,x}(t')\rangle + \langle F_{I,x}(t)F_{I,x}(t')\rangle + \alpha^2 D^2(\langle F_{h,y}(t)F_{h,y}(t')\rangle + \langle F_{I,y}(t)F_{I,y}(t')\rangle)}{(G^2 + \alpha^2 D^2)^2}$$

$$= \frac{G^2(\langle F_{h,x}(t)F_{h,x}(t')\rangle + \langle F_{I,x}(t)F_{I,x}(t')\rangle + \alpha^2 D^2(\langle F_{h,y}(t)F_{h,y}(t')\rangle + \langle F_{I,y}(t)F_{I,y}(t')\rangle)}{(G^2 + \alpha^2 D^2)^2}$$

$$= \frac{G^2(\langle F_{h,x}(t)F_{h,x}(t)F_{h,x}(t')\rangle + \langle F_{I,x}(t)F_{I,x}(t')\rangle + \alpha^2 D^2(\langle F_{h,y}(t)F_{h,y}(t')\rangle + \alpha^2 D^2\langle F_x(t)F_x(t')\rangle}{(G^2 + \alpha^2 D^2)^2}$$

$$= \frac{G^2(\langle F_{h,x}(t)F_{h,x}(t)F_{h,x}(t')\rangle + \langle F_{I,x}(t)F_{I,x}(t')\rangle + \alpha^2 D^2(\langle F_{h,y}(t)F_{h,y}(t')\rangle + \langle F_{I,y}(t)F_{I,y}(t')\rangle}{(G^2 + \alpha^2 D^2)^2}$$

$$= \frac{G^2(\langle F_{h,x}(t)F_{h,x}(t)F_{h,x}(t')\rangle + \langle F_{I,x}(t)F_{I,x}(t')\rangle + \alpha^2 D^2(\langle F_{h,y}(t)F_{h,y}(t')\rangle + \langle F_{I,y}(t)F_{I,y}(t')\rangle}{(G^2 + \alpha^2 D^2)^2}$$

$$= \frac{G^2(\langle F_{h,x}(t)F_{h,x}(t)F_{h,x}(t')\rangle + \langle F_{I,x}(t)F_{h,x}(t')\rangle + \alpha^2 D^2(\langle F_{h,x}(t)F_{h,y}(t')\rangle + \langle F_{I,y}(t)F_{h,y}(t')\rangle}{(G^2 + \alpha^2 D^2)^2}$$

$$= \frac{G^2(\langle F_{h,x}(t)F_{h,x}(t)F_{h,x}(t)F_{h,x}(t)F_{h,x}(t)F_{h,x}(t)F_{h,x}(t)}) + \alpha^2 D^2(\langle F_{h,$$

The time integration $R_x = \int_0^t v_x(t')dt'$ yields the mean squared displacements:

$$\langle R_x^2(t)\rangle = \langle R_y^2(t)\rangle = 2\mathcal{D}t = \frac{\alpha D\left(2k_BT + (1+\beta^2)\frac{\delta\varepsilon}{E_F}(eV\coth\frac{eV}{2k_BT} - 2k_BT)\right)}{G^2 + \alpha^2D^2}t,\tag{30}$$

The diffusion relations for skyrmion (30) correspond to the known results [54, 55] (equilibrium case) in the absence of an external current source at $V \to 0$.

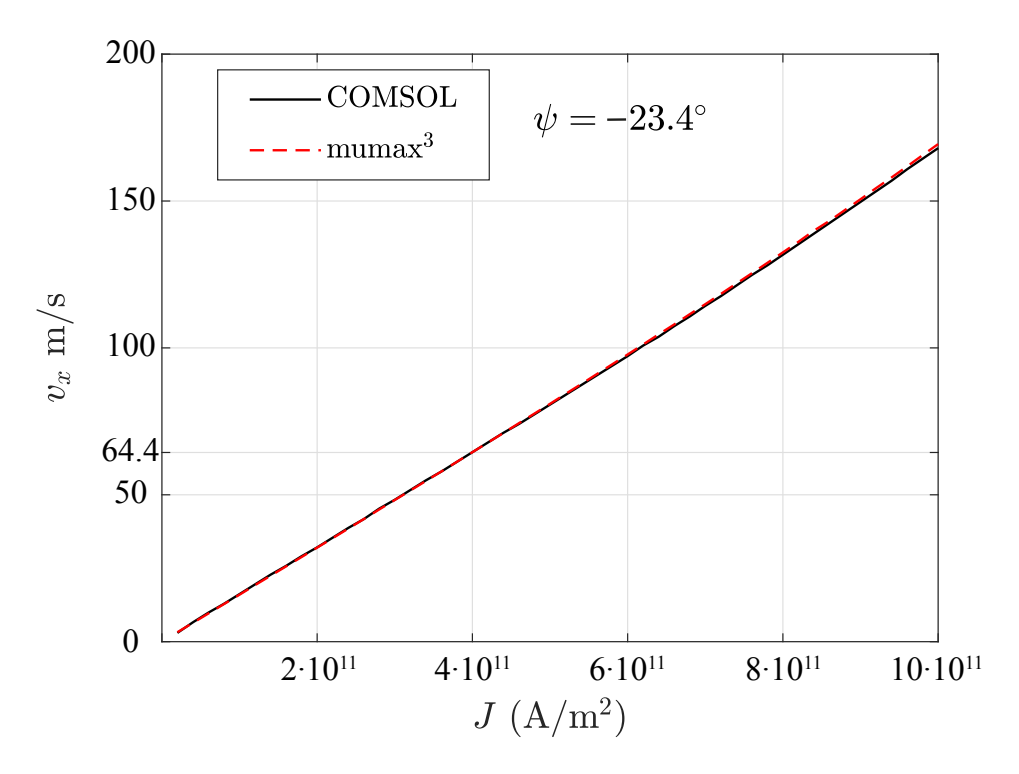


FIG. 3. Velocity of skyrmion v_x versus current density J obtained in COMSOL Multiphysics (black solid line) and mumax³ (red dotted line).

III. MICROMAGNETIC SIMULATION

Micromagnetic simulation were performed with COMSOL Multiphysics using the micromagnetic module [56, 57] for two-dimensional system. This multiphysics platform allows for the generalization of the LLG equations by incorporating additional nonequilibrium fluctuation terms. The ability to extend the functionality of the standard micromagnetic model is particularly relevant for studying integrated systems. Next, we will make the transition from the units of measurement of the parameters of micromagnetic modeling in COMSOL to the units of the generally accepted open platform mumax³. Effective field in mumax³ has the form:

$$\mathbf{H}_{\text{eff}} = \frac{2A_{\text{ex}}}{M_s} \nabla^2 \mathbf{m} + \frac{2K_u}{M_s} m_z \mathbf{e}_z + \frac{2D_{\text{DMI}}}{M_s} (\nabla m_z - (\nabla \cdot \mathbf{m}) \mathbf{e}_z), \ [T].$$
 (31)

Effective field in COMSOL Multiphysics is:

$$\frac{\mathbf{H}_{\text{eff}}}{\mu_0} = A'_{\text{ex}} \nabla^2 \mathbf{m} + K'_u m_z \mathbf{e}_z - D'_{\text{DMI}} (\nabla m_z - (\nabla \cdot \mathbf{m}) \mathbf{e}_z), \text{ [Am}^{-1}].$$
(32)

In the main text of the paper, we use the parameter terminology adopted for mumax³. Consequently, the relationship between the coefficients for the two approaches to micromagnetic modeling is

$$A'_{\text{ex}} = \frac{2A_{\text{ex}}}{M_s \mu_0}, \quad K'_{\text{u}} = \frac{2K_{\text{ex}}}{M_s \mu_0}, \quad D'_{\text{DMI}} = \frac{2D_{\text{DMI}}}{M_s \mu_0}.$$
 (33)

We used the following parameters in our simulations: the exchange coefficient $A_{\rm ex}=10^{-11}$ J/m, the anisotropy $K_u=10^6$ J/m³, the saturation magnetization $M_s=0.6\cdot 10^6$ A/m, the interfacial DMI coefficient $D_{\rm DMI}=-3.5\cdot 10^{-3}$ J/m² and the damping parameters $\alpha=\beta=0.3$. The racetrack sample has (x-y) plane section of 500×150 nm² and thickness $\Delta_f=1$ nm. Electric current is $J=4\cdot 10^{11}$ A/m², applied voltage is U=0.5 V and temperature is T=300 K. Such parameters are typical for the experiments on the racetracks [16, 45, 46]. The topological properties of skyrmions can be completely characterized by three different numbers (Q,Q_v,Q_h) denoting the topological charge, vorticity number and helicity number, respectively [59, 60]. We restrict ourselves to the DMI, which leads to stable Néel-type skyrmions $(1,1,\pi)$.

Next, we compare both approaches to micromagnetic modeling using the COMSOL Multiphysics and mumax³ platforms for the above system parameters. As shown in Fig. 3, good agreement was obtained between the skyrmion velocities v on the racetrack as functions of current density J. It is also worth noting that the simulation was performed for skyrmion dynamics with suppression of the skyrmion Hall effect, which corresponds to a polarization angle of $\psi = -23.4^{\circ}$. The obtained results indicate the equivalence of both micromagnetic modeling approaches based on both COMSOL Multiphysics and mumax³ platforms.

Once we have determined all the modeling parameters, we can calculate the necessary quantities included in the Thiele equations.

$$G = \frac{M_s \Delta_f}{\gamma} \int \mathbf{m} \cdot [\nabla_x \mathbf{m} \times \nabla_y \mathbf{m}] dx dy = 4\pi M_s \Delta_f / \gamma = 4.29 \cdot 10^{-14} \ [kg/s],$$

$$D = \frac{M_s \Delta_f}{\gamma} \int \nabla_x \mathbf{m} \cdot \nabla_x \mathbf{m} dx dy = 18.1 M_s \Delta_f / \gamma = 6.17 \cdot 10^{-14} \ [kg/s],$$

$$\langle v_x \rangle \approx \frac{-GF_{\text{SOT},y} - \alpha DF_{\text{SOT},x}}{G^2 + \alpha^2 D^2} = \frac{Pj\hbar}{2e} \cdot \frac{-G\int [\nabla_y \mathbf{m} \times \mathbf{m}] \cdot \mathbf{p} dx dy - \alpha D\int [\nabla_x \mathbf{m} \times \mathbf{m}] \cdot \mathbf{p} dx dy}{G^2 + \alpha^2 D^2} = 64.4 \ [m/s],$$

$$\langle v_y \rangle \approx \frac{GF_{\text{SOT},x} - \alpha DF_{\text{SOT},y}}{G^2 + \alpha^2 D^2} = \frac{Pj\hbar}{2e} \cdot \frac{G\int [\nabla_x \mathbf{m} \times \mathbf{m}] \cdot \mathbf{p} dx dy - \alpha D\int [\nabla_y \mathbf{m} \times \mathbf{m}] \cdot \mathbf{p} dx dy}{G^2 + \alpha^2 D^2} = 0.$$
(34)

Here $\langle v_y \rangle$ and $\langle v_y \rangle$ depend mainly on the force induced by Slonczewski's torque term $F_{\text{SOT},i} = \frac{P_j \hbar}{2e} \int \left[\nabla_i \mathbf{m} \times \mathbf{m} \right] \cdot \mathbf{p} dx dy$ and negligibly on $F_{\text{eff},i}$. It should also be noted that \mathbf{m} in the integral represents the magnetization field distribution for an equilibrium isolated skyrmion on a given racetrack.

IV. FIRST PASSAGE TIME MOMENTS OF STOCHASTIC EQUATIONS

Application of the Thiele approach to the LLG equation with noise terms leads to a system of two independent stochastic equations with constant coefficients:

$$d\mathbf{R} = \langle \mathbf{v} \rangle dt + \boldsymbol{\xi} \sqrt{2\mathcal{D}dt}. \tag{35}$$

Here, $\langle \mathbf{v} \rangle$ is the drift velocity, $\boldsymbol{\xi} = (\xi_1, \xi_2)^T$ is a random vector with normal distribution, were $\langle \xi_1 \rangle = \langle \xi_2 \rangle = 0$ and $\langle \xi_1 \xi_2 \rangle = 0$. This stochastic equation describes the classical diffusion process with drift and has a well-known analytical solution [63]. The first two non-zero moments of \mathbf{R} are the mean value $\langle \mathbf{R} \rangle = \langle \mathbf{v} \rangle t$ and variance $\langle \delta \mathbf{R}^2 \rangle = \langle \delta R_x^2 \rangle + \langle \delta R_y^2 \rangle = 4\mathcal{D}t$.

We treat the first-passage-time problem componentwise. For each component, the moments of the first passage time τ to an absorbing boundary satisfy the standard hierarchy of ODEs derived from the backward Kolmogorov equation (see §5.10 in [63]):

$$\mathcal{D}\frac{\mathrm{d}^2}{\mathrm{d}\lambda^2}\langle\tau_n(\lambda)\rangle + \langle v_\lambda \rangle \frac{\mathrm{d}}{\mathrm{d}\lambda}\langle\tau_n(\lambda)\rangle = -n\langle\tau_{n-1}(\lambda)\rangle \tag{36}$$

Here $\lambda = \{x,y\}$, $\langle \tau_n(\lambda) \rangle$ is n-th moment of the first passage time τ , \mathcal{D} is the diffusion coefficient and $\langle v_{\lambda} \rangle$ is the drift velocity along λ -axis. The variable λ belongs to the range $\lambda_a \leq \lambda \leq \lambda_b$ with absorbing boundaries at the points λ_a and λ_b , which correspond to the conditions $\langle \tau_n(y) \rangle|_{y=\lambda_a} = \langle \tau_n(y) \rangle|_{y=\lambda_b} = 0$. Using zero-moment equality $\langle \tau_0(\lambda) \rangle = 1$, one has the following system of equations for the first two moments:

$$\begin{cases} \mathcal{D} \frac{\mathrm{d}^2}{\mathrm{d}\lambda^2} \langle \tau_1(\lambda) \rangle + \langle v_\lambda \rangle \frac{\mathrm{d}}{\mathrm{d}\lambda} \langle \tau_1(\lambda) \rangle = -1 \\ \mathcal{D} \frac{\mathrm{d}^2}{\mathrm{d}\lambda^2} \langle \tau_2(\lambda) \rangle + \langle v_\lambda \rangle \frac{\mathrm{d}}{\mathrm{d}\lambda} \langle \tau_2(\lambda) \rangle = -2 \langle \tau_1(\lambda) \rangle \end{cases}$$
(37)

which can be easily solved with specified boundary conditions for constant \mathcal{D} and $\langle v_{\lambda} \rangle$.

We set the x-axis to run along the racetrack, with width 2a. Skyrmions are initialized at the center of the racetrack, defined as the origin of the coordinate system, and possess a drift velocity $\langle v \rangle$ along the racetrack.

For the problem of first passage time τ to the side racetrack boundary, we have $\langle v_y \rangle = 0$, and the boundary conditions $\langle \tau_{1,2}(y) \rangle|_{y=-a} = \langle \tau_{1,2}(y)|_{y=a} \rangle = 0$. In this case, the solution of the system (37) leads to the following expressions for the mean $\langle \tau_y \rangle$ and the standard deviation $\langle \sigma_y \rangle$ of FPT from the center of the racetrack to side boundary:

$$\langle \tau_y \rangle = \langle \tau_1(y) \rangle|_{y=0} = \frac{a^2}{2\mathcal{D}}$$

$$\langle \sigma_y \rangle = \sqrt{\langle \tau_2(y) \rangle|_{y=0} - (\langle \tau_1(y) \rangle|_{y=0})^2} = \frac{a^2}{\sqrt{6}\mathcal{D}}$$
(38)

For the case of first passage time τ along the racetrack to the detection area at a distance d, we have $\langle v_x \rangle = \langle v \rangle$, and the boundary conditions $\langle \tau_{1,2}(x) \rangle|_{x=-\infty} = \langle \tau_{1,2}(x)|_{x=d} \rangle = 0$. In that case, the mean $\langle \tau_x \rangle$ and the standard deviation $\langle \sigma_x \rangle$ of FPT to the detection area of the racetrack read as:

$$\langle \tau_x \rangle = \langle \tau_1(x) \rangle|_{x=0} = \frac{d}{\langle v \rangle},$$

$$\langle \sigma_x \rangle = \sqrt{\langle \tau_2(x) \rangle|_{x=0} - (\langle \tau_1(x) \rangle|_{x=0})^2} = \sqrt{\frac{2\mathcal{D}d}{\langle v \rangle^3}}.$$
(39)